PCCP

PAPER

View Article Online
View Journal | View Issue

Cite this: *Phys. Chem. Chem. Phys.*, 2025, **27**, 16664

Angle-dependent electrocatalytic activity of twisted bilayer graphene for the hydrogen evolution reaction†

Lifang Chen, [a] Jin Li [ab] and Xi Yin *[a]

Received 15th April 2025,
Accepted 7th July 2025

DOI: 10.1039/d5cp01437a

rsc.li/pccp

Two-dimensional (2D) materials are attractive for their unique electronic structures and electrocatalytic properties. In this work, we propose to use the twist angle as a knob to tune the electrocatalytic properties of 2D materials. As proof of concept, we investigate the effects of twist angle (>10°) on the electrocatalytic properties of twisted bilayer graphene (tBLG). We predict the activity of tBLG with the twist angle of 13.174° and 21.787° for the hydrogen evolution reaction (HER) using a density functional theory (DFT) calculation and computational hydrogen electrode (CHE) approach. We calculate the hydrogen adsorption energy (ΔG_{H^*}) at various sites on tBLG and examine their angle-dependency. By comparing the ΔG_{H^*} for different active sites of untwisted bilayer graphene (BLG) and tBLG, we find that the ΔG_{H^*} decreases with the increase of the twist angle. As a result, the thermodynamic limiting potential for the HER increases with the twist angle. Furthermore, the ΔG_{H^*} shows a correlation with the layer distance ($\bar{d}$) and the site location on the 2D plane. Detailed analysis reveals that the twist of bilayer graphene could increase the z height (d_z) of the active sites as a function of their distance to the symmetry centers, alter the local geometry of the active sites, and therefore modify the ΔG_{H^*}. These results indicate that the twist angle can be effectively used as a knob to fine-tune the electrocatalytic properties of 2D materials.

1. Introduction

Two-dimensional (2D) materials are promising electrocatalysts with their advantages of ultra-thin layered structure, large specific surface area, high density of surface active sites, and fast charge transmission.[1–9] Among the 2D materials, graphene,[10–12] nitrogen-doped carbon,[13–16] metal halogens,[17,18] and layered double hydroxides[19,20] have received great attention for their unique electrocatalytic properties. Various structural and compositional strategies, such as elemental doping, defect engineering, ligand modification, spin state tunning, and van der Waals (vdW) heterostructures, have been developed to improve their electrocatalytic activity.[4,13,21–27] Recently, physicists revealed that twisted 2D materials possess exceptional traits like unconventional superconductivity,[28,29] and orbital magnetism.[28,30] This exciting finding leads us to speculate whether the twisted 2D materials may have unique chemical and thermodynamic properties that differ from their untwisted counterparts. The twist angles of layered 2D materials may alter the interaction between the reactants and the catalytic sites on 2D materials at different degrees depending on the twist angle of adjacent layers, eventually leading to angle-dependent electrocatalytic properties. Thus, the twist angles of layered 2D materials can potentially be used as a novel knob to tune their catalytic properties. This new strategy is worth exploring, as it may lead to surprising discoveries.

Twisted bilayer graphene (tBLG) exhibits remarkably diverse electronic properties that evolve non-monotonically with rotation angle. This angle-dependent behavior manifests in three distinct regimes: at small twist angles ($\theta < 3^\circ$), long-range moiré superlattices dominate, generating flat electronic bands and correlated quantum states.[29] In the intermediate regime ($3^\circ \leq \theta \leq 10^\circ$), expanding AA-stacking domains create heterogeneous electronic environments with localized states and stacking-dependent interlayer distances.[31] At large twist angles ($\theta > 10^\circ$), unique symmetry features are retained.

Herein, we use the hydrogen evolution reaction (HER) as a model reaction to investigate the origin of the angle-dependent electrocatalytic activity of twisted bilayer graphene (tBLG) at twist angle >10°. The HER could be considered as the simplest electrochemical reaction and the foundation of multiple electron-proton transfer reactions.[32,33] The hydrogen adsorption

[a] State Key Laboratory of Coal Conversion, Institute of Coal Chemistry, Chinese Academy of Sciences, Taiyuan, Shanxi 030001, China. E-mail: xiyin@sxicc.ac.cn
[b] College of Chemical Engineering and Technology, Taiyuan University of Science and Technology, Taiyuan, Shanxi 030024, China

† Electronic supplementary information (ESI) available. See DOI: https://doi.org/10.1039/d5cp01437a

free energy (ΔG_{H^*}) at all on-top sites of untwisted bilayer graphene (BLG) and tBLG with twist angles of θ = 13.174° and 21.787° is meticulously calculated and examined for their angle-dependency. The results demonstrate that the ΔG_{H^*} decreases with the increase of the twist angle, and the U_L for the HER increases with the twist angle. And the ΔG_{H^*} varies as a function of the site position parameters on the 2D plane, including the z-distance to the bottom layer and distance to the high-symmetry centers. Consequently, the twist of bilayer graphene alters the local geometry of the active sites, thereby modifying the ΔG_{H^*}. This work provides a helpful footstone for further broadening the application of twisted 2D materials for catalysis.

2. Models and methods

2.1. Models of twisted bilayer graphene

There are three types of high-symmetry stacking structures for bilayer graphene, namely AB-, AA-, and saddle-point (SP-) stacking configurations, as shown in Fig. 1a.[34] Each configuration has two high-symmetry twist centers, **1** and **2**. We construct the models of tBLG by twisting one constituent lattice in the AB stacking configuration around center **1** (Fig. 1b). The unit cell of a high-symmetry tBLG has two basis vectors $\mathbf{A}_1 = m\mathbf{a}_1 + n\mathbf{a}_2$ and $\mathbf{A}_2 = -n\mathbf{a}_1 + (m+n)\mathbf{a}_2$, where $\mathbf{a}_1$ and $\mathbf{a}_2$ are the basis vectors of the untwisted BLG lattice, and m and n are coprime indices.[35] Table S1 (ESI†) summarizes the coprime indices, θ, and the number of atoms in the primitive cells of high-symmetry tBLG. Considering the computational cost of the density functional theory (DFT) calculation and the complexity/specificity of models and electronic structures, we first focus on the tBLG at twist angle >10°, specifically θ = 13.174° and θ = 21.787°, namely tBLG (13.174°) and tBLG (21.787°).

For comparison, we redefine two unit cells of the BLG lattice (θ = 0°) to include the same number of C atoms as their tBLG counterparts, namely BLG-28(0°) and BLG-76(0°). Using the unit cells of tBLG and BLG of the same C atom numbers ensures the modeling of H adsorption at the same H-coverage. A vacuum space of 20 Å along the z direction was added to avoid interactions between adjacent slabs.

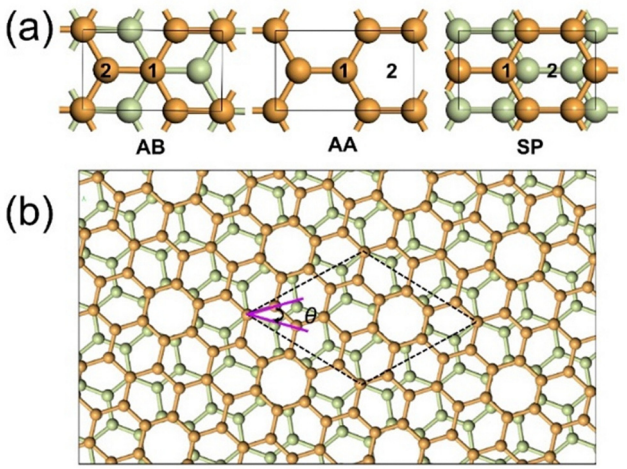

Fig. 1 (a) Three types of high-symmetry bilayer graphene (BLG) in AB-, AA-, and saddle-point (SP-) stacking configurations. (b) Twist angle (θ) is produced by twisting one constituent lattice of BLG in the AB-stacking configuration.

2.2. Methods

Structure optimization and energy calculation were performed by the Vienna *ab initio* simulation package (VASP 5.4.4).[36,37] The core-electron and exchange–correlation interactions were described by the Perdew–Burke–Ernzerhof (GGA-PBE) functional[38] with the projector-augmented-wave (PAW)[39,40] pseudopotential. To consider the van der Waals interaction, Grimme's DFT-D3 was utilized.[41] A cut-off energy of 400 eV was set for the plane wave basis. The Monkhorst–Pack k-point mesh 3 × 3 × 1 was employed for all BLG and tBLG models. The structure optimization was completed until the forces and energies were less than 0.02 eV Å^{-1} and 10^{-5} eV per atom, respectively.

The calculation of the H adsorption free energy was performed by using the computational hydrogen electrode (CHE) approach.[42] In this framework, the free energy of the electron–proton pair ($H^+ + e^-$) can be referenced to the chemical potential of gaseous H_2 at equilibrium (0 V *vs.* standard hydrogen electrode). The H adsorption energy can be computed using the following eqn (1) and (2):

$$\Delta E_{H^*} = E_{H^*} - E_* - 1/2E_{H_2(g)} \quad (1)$$

$$\Delta G_{H^*} = \Delta E_{H^*} + \Delta E_{ZPE} + \Delta U(T) - T\Delta S \quad (2)$$

where E_{H^*} is the electronic energy after H adsorption; E_* is the electronic energy of the clean surface; $E_{H_2(g)}$ denotes the electronic energy of gaseous H_2; ΔE_{H^*} is the electronic energy difference after and before adsorption of H; ΔE_{ZPE} is the change of zero-point energy; $\Delta U(T)$ is the change of internal energy; T is temperature (T = 298.15 K), and ΔS is the entropy change (T = 298.15 K).

The thermodynamic limiting potential is calculated using eqn (3):

$$U_L = -|\Delta G_{H^*}| \quad (3)$$

3. Results and discussion

Fig. 2 shows optimized structures for untwisted bilayer graphene (BLG-76 and BLG-28) and twisted bilayer graphene (tBLG) with θ of 13.174° and 21.787°. After twisting the upper layer by θ = 13.174° and 21.787°, the average distance in the z-direction between the top and bottom layer atoms ($\bar{d}$) increases from 3.492 Å (0°) to 3.564 Å (13.174°) by 2.06% and 3.523 Å (21.787°) by 0.89%, indicating that the twist destabilizes the bilayer structure slightly. The surface structure of the BLG and tBLG differs significantly and the on-top adsorption sites can be categorized into various types based on their local geometry and symmetry. Two types of on-top H-adsorption sites are identified on the BLG surface (Fig. 2a and c) while more types of unique sites form at the tBLG surfaces due to the twist of the upper layer (Fig. 2b and d). Both tBLG(13.174°) and

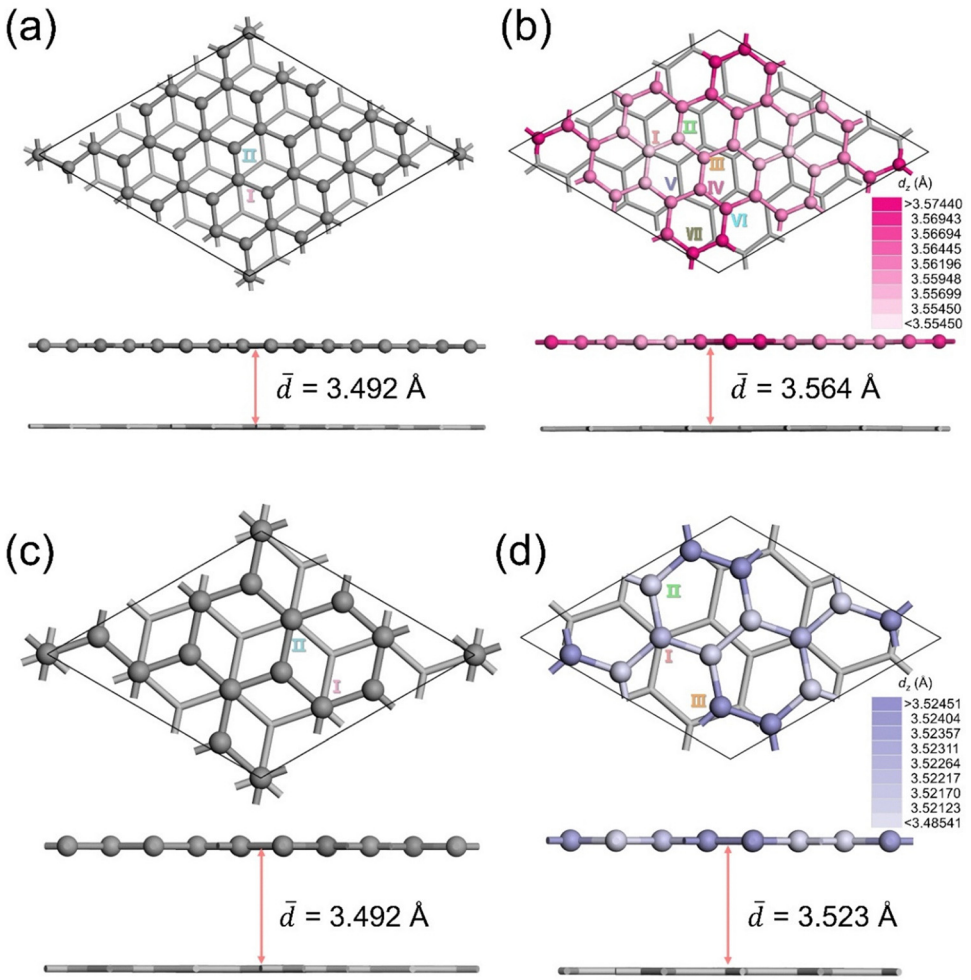

Fig. 2 Optimized structures and the active sites of (a) BLG-76(0°), (b) tBLG(13.174°), (c) BLG-28(0°), and (d) tBLG(21.787°) and the mapping of d_z. Color bar stands for d_z values. $\bar{d}$ stands for the difference between average z-distance of the top and bottom layer atoms.

tBLG(21.787°) have a space group $P3$ symmetry, including two types of symmetry centers C1 and C2 (Fig. S1, ESI†). To clarify the adsorption site classification and spatial distribution around the C1/C2 centers, high-symmetry adsorption sites are defined relative to C1/C2. C1-centered sites: directly atop the moiré hollow (AA-stacked regions); C2-centered sites: near stacking-domain boundaries (AB/BA transitions). And the H-adsorption sites are arranged in three-phases and repeated every 120° with the three-fold rotational axis shown as triangles. After twist of the upper surface, the number of types of sites increases from two to seven (θ = 13.174°) and three (θ = 21.787°), respectively. The z-distance (d_z) of the active site relative to the bottom layer is calculated by:

$$d_z = z_{i\text{-top}} - \bar{z}_{\text{bottom}} \quad (4)$$

where $z_{i\text{-top}}$ is the z-height of the active site in the top layer, and $\bar{z}_{\text{bottom}}$ is the average z-height of the bottom layer atoms. The d_z for each type of site varies on the 2D plane as a function of their relative position to the C1 and C2 symmetry centers, as shown in Fig. 2b and d. The sites are colored in different saturation levels to show the change of d_z, indicating a change in the geometric structure of the sites. The d_z increases slightly as the active site locates further away from the C1 to C2 center. For tBLG with θ = 13.174° and 21.787°, the d_z increases from 3.555 to 3.574 Å and from 3.521 to 3.525 Å, respectively. These active sites with varied local geometry could lead to diverse performances for the hydrogen evolution reaction.

The adsorption energy of hydrogen atoms at the active site (ΔG_{H^*}) has been proven to be a suitable activity descriptor for a broad range of HER catalysts, including both metal-based and metal-free materials.[42,43] We modeled the structures for H adsorbed at the two sites of BLG and the ten sites of tBLG. Fig. 3a–d show the color rendered mapping of ΔG_{H^*} on tBLG and BLG (detailed structures and values are shown in Fig. S2 and S3, ESI†). The color from dark to bright represents the ΔG_{H^*} from low to high, corresponding to H-binding from strong to weak. For tBLG(21.787°) and tBLG(13.174°), site II adjacent to the C1 center exhibits the highest ΔG_{H^*}. The ΔG_H of the sites except that on the C1 center decreases as the site is further away from the C1 center and closer to the C2 center. (The difference in ΔG_{H^*} for various sites is significant and larger than the precision from the DFT calculation with a STD

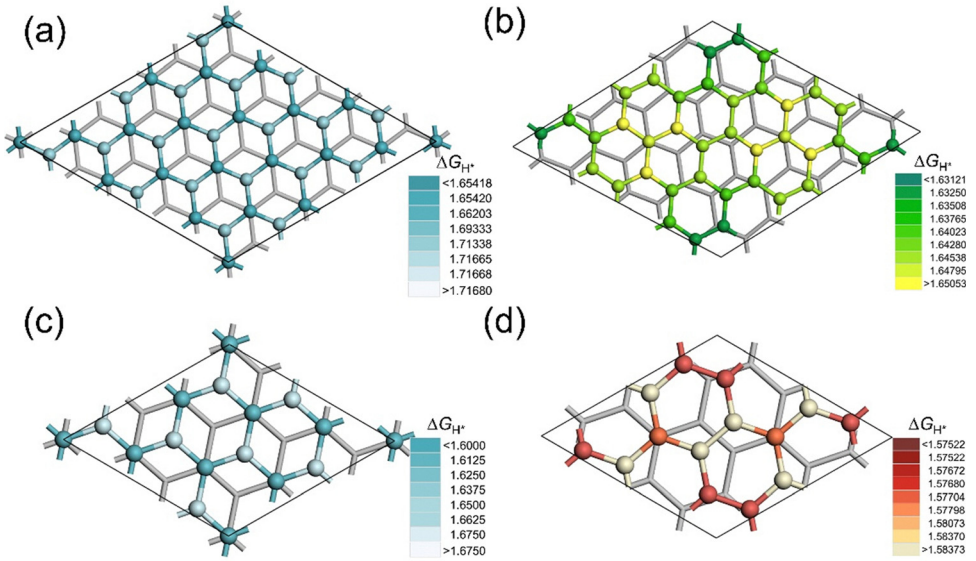

Fig. 3 The energy-site relationship mapping for (a) BLG-76 (0°), (b) tBLG(13.174°), (c) BLG-28(0°), and (d) tBLG(21.787°). Color bar stands for H adsorption free energy value.

of 0.001 eV in Table S2 (ESI†).) Fig. 4a and b show the linear correlation between the bilayer distance of each site and ΔG_{H^*}. As d_z increases, the corresponding sites ΔG_{H^*} decrease. Fig. 4c and d show the location-dependency of ΔG_{H^*} and d_z of the sites in the 2D plane of tBLG, in which the atoms closer to the C1 center have higher ΔG_{H^*} and shorter d_z. Moreover, compared with BLG, the $\bar{d}$ in tBLG increases with twist angle (Fig. 2 and 3), corresponding to the decreased ΔG_{H^*} (average value). Therefore, increased z-distance (*e.g.*, at AA-stacked regions) reduces the interlayer orbital overlap, weakens sp^2–sp^2 hybridization, and enhances p_z-orbital availability for H adsorption. Furthermore, Fig. S4 (ESI†) compares the ΔG_{H^*} for the single monolayer graphene (MLG), BLG, and tBLG. The ΔG_{H^*} increases monotonically from MLG to BLG but decreases in tBLG. These

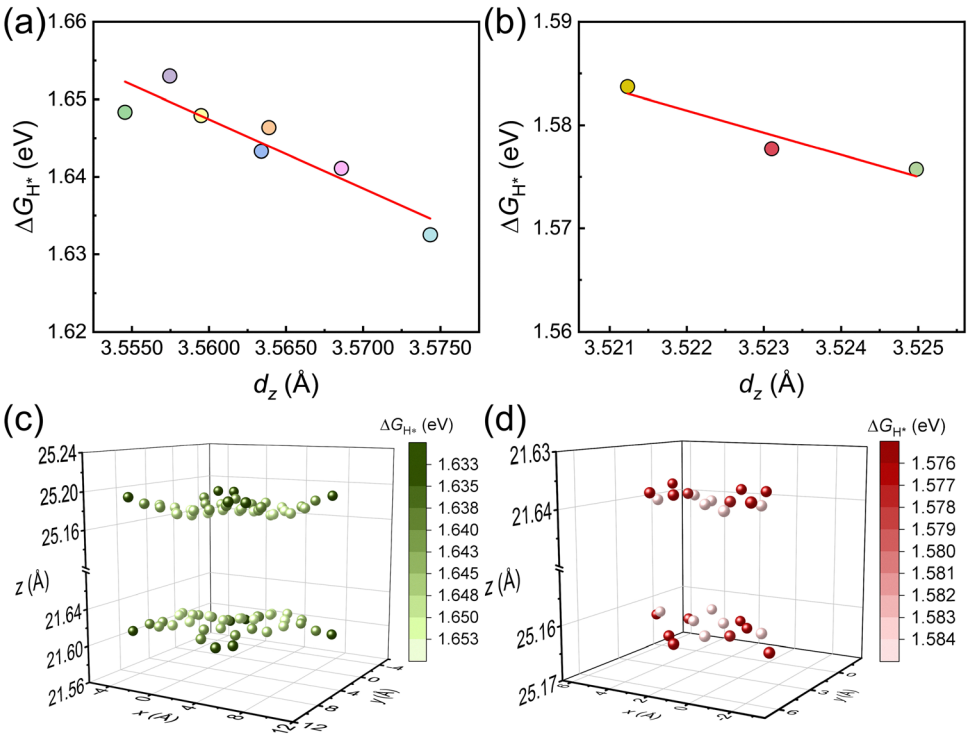

Fig. 4 Correlation between the d_z and ΔG_{H^*} for (a) tBLG(13.174°) and (b) tBLG (21.787°). Points with different colors represent various active sites. 3D scatter plots of the relationship between the atom position and ΔG_{H^*} for (c) tBLG(13.174°) and (d) tBLG(21.787°). The color gradient represents ΔG_{H^*}.

results indicate that interlayer coupling in BLG weakens the binding strength, while the introduction of a twist angle further modulates the coupling, ultimately enhancing the binding strength.

Fig. 5a shows the relationship between twist angle and ΔG_{H^*}. The average of ΔG_{H^*} was presented by the saturated point. From $\theta = 0^\circ$ to 13.174° and $\theta = 0^\circ$ to 21.787°, ΔG_{H^*} has obviously decreased. The $\Delta\Delta G_{H^*}$ is used to further quantify the change of ΔG_{H^*} with twist angle:

$$\Delta\Delta G_{H^*} = \Delta G_{H^*}(\theta) - \Delta G_{H^*}(0^\circ) \quad (5)$$

The average $\Delta\Delta G_{H^*}$ decreases from -0.041 eV to -0.061 eV when θ increases from 13.174° to 21.787° (Fig. 5b), indicating that the larger twisted angle leads to a larger change of ΔG_{H^*}. Fig. 5c shows the reaction free energy diagram for the HER at different sites. Based on the Sabatier principle, the binding of atomic H to an effective HER catalyst should neither be too strong nor too weak. Consequently, smaller $|\Delta G_{H^*}|$ values represent a lower thermodynamic barrier for the HER. For an ideal HER catalyst, the ΔG_{H^*} should be 0 eV. The positive values of ΔG_{H^*} represents the under-binding of the H* intermediate and are the origin of the thermodynamic overpotential. The lower ΔG_{H^*} values on tBLG than on BLG indicate that twist angle promotes the HER activity. The thermodynamic limiting potential (U_L) is calculated using eqn (3). Correspondingly, the U_L for the HER also increases with the twist angle (Fig. 5d). We also considered the electronic structure effect on the HER (Fig. S5 and S6, ESI†), but found that the charge density difference almost has no difference between BLG and tBLG surfaces. This might be caused by the weak interaction in bilayer graphene. Notably, no significant correlation emerged between the Bader charge of the active sites and ΔG_{H^*} as demonstrated in Fig. S7a and b (ESI†). Additional insights were gained from projected density of states (PDOS) calculations comparing the BLG and tBLG configurations (Fig. S7c and d, ESI†). The twist induced a distinct change in electronic structure, manifested by a reduction in the number of peaks at the Fermi level from three to one following twisting. But the corresponding p band center of site-PDOS lacks clear correlation with adsorption energy trends across different configurations (Fig. S7e and f, ESI†). Therefore, correlation analyses reveal that geometric parameters outperform local electronic descriptors (Bader charge or PDOS) in predicting site-adsorption energies. The twist angle generates various active site structures and increases the bilayer distance, further enhancing the HER activity.

4. Conclusion

We scrutinized the angle-dependent electrocatalytic activity of the twisted bilayer graphene (tBLG) with twist angles greater than 10° for the HER using DFT calculations and the CHE

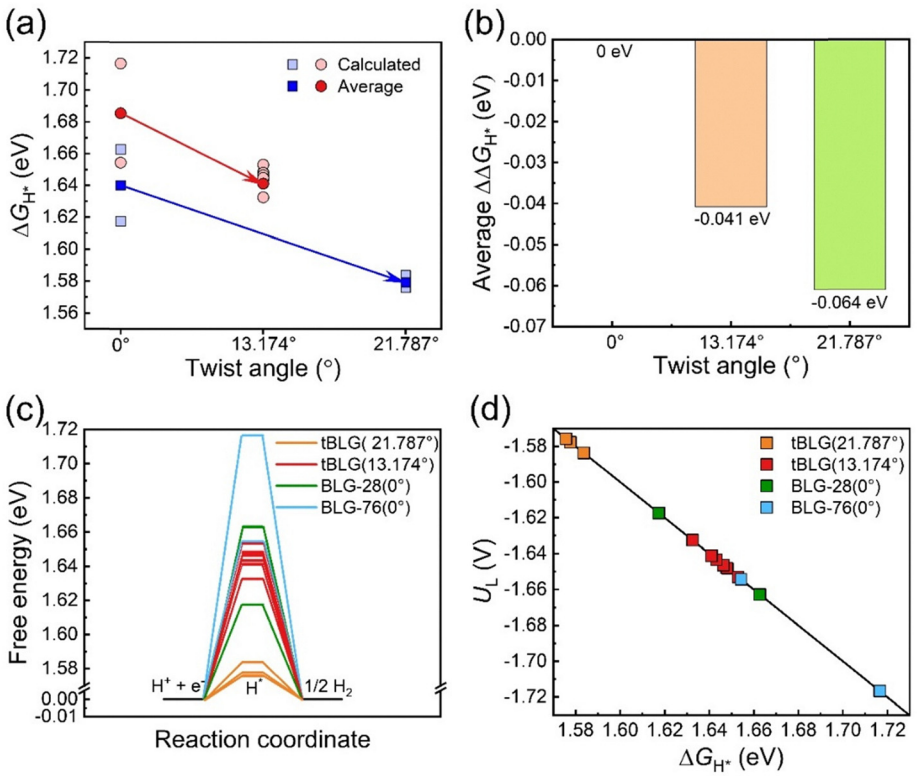

Fig. 5 (a) Dependence of ΔG_{H^*} on the twist angle. Saturated points represent the average values of ΔG_{H^*}; unsaturated points show individual calculated ΔG_{H^*} values. Red data points correspond to the ΔG_{H^*} values for tBLG(13.174°); blue data points represent ΔG_{H^*} values for tBLG(21.787°). (b) Average $\Delta\Delta G_{H^*}$ as a function of the twist angle. (c) Free energy diagram of the HER at various sites of the tBLG and BLG surface. (d) Thermodynamic limiting potentials (U_L) of the HER as a function of ΔG_{H^*}.

approach. The results show that the twisting of BLG leads to an increase in the bilayer distance, which follows a decreasing trend as the site is located further away from the C1 to C2 symmetry center. Meanwhile, the intensity of hydrogen adsorption also varies as a function of site position in the 2D plane, and the ΔG_{H^*} decreases as the d_z of the active site increases. Both d_z and ΔG_{H^*} correlate within the 2D plane of tBLG, which is attributed to the local geometry in the tBLG structures generated by the twist. This effect is further enhanced with the increase of the the twist angle. As a result, twisting the BLG results in the 2D position-dependency of various active sites with unique local structures and fine-tuned HER activities. This study suggests that twisting can be a novel strategy to design 2D materials with precisely controlled catalytic activities.

Author contributions

Lifang Chen: investigation, methodology, writing – original draft, visualization. Jin Li: investigation. Xi Yin: conceptualization, investigation, writing – review & editing, supervision, funding acquisition.

Conflicts of interest

The authors declare no competing financial interest.

Data availability

All the data are available in the main text and the ESI.†

Acknowledgements

Financial support from the State Key Laboratory of Coal Conversion, Institute of Coal Chemistry, Chinese Academy of Sciences is greatly appreciated. This study was financially supported by Shanxi Province Youth Natural Science Foundation Grant No. 202103021223458, and Shanxi Province Grant No. 2023SHB003. The authors would like to thank Dr Xiaodong Wen and Dr Xingchen Liu at ICC CAS for their support for calculations during the project.

References

1 S. Yu, C. Zhang and H. Yang, *Chem. Rev.*, 2023, **123**, 3443–3492.
2 K. Wan, T. Chu, B. Li, P. Ming and C. Zhang, *Adv. Sci.*, 2023, **10**, e2203391.
3 X. Liu and L. Dai, *Nat. Rev. Mater.*, 2016, **1**, 16064.
4 Q. Zhu, Y. Qu, D. Liu, K. W. Ng and H. Pan, *ACS Appl. Nano Mater.*, 2020, **3**, 6270–6296.
5 A. VahidMohammadi, J. Rosen and Y. Gogotsi, *Science*, 2021, **372**, eabf1581.
6 Y. Wang, H. Su, Y. He, L. Li, S. Zhu, H. Shen, P. Xie, X. Fu, G. Zhou, C. Feng, D. Zhao, F. Xiao, X. Zhu, Y. Zeng, M. Shao, S. Chen, G. Wu, J. Zeng and C. Wang, *Chem. Rev.*, 2020, **120**, 12217–12314.
7 X. Yin, M. Shi, K. S. Kwok, H. Zhao, D. L. Gray, J. A. Bertke and H. Yang, *Nano Res.*, 2018, **11**, 3442–3452.
8 Y. T. Pan, X. Yin, K. S. Kwok and H. Yang, *Nano Lett.*, 2014, **14**, 5953–5959.
9 X. Yin, X. Liu, Y.-T. Pan, K. A. Walsh and H. Yang, *Nano Lett.*, 2014, **14**, 7188–7194.
10 Q. Wan, H. Guo and S. Lin, *ACS Catal.*, 2022, **12**, 14601–14608.
11 Y. Qu, Y. Ke, Y. Shao, W. Chen, C. T. Kwok, X. Shi and H. Pan, *J. Phys. Chem. C*, 2018, **122**, 25331–25338.
12 R. Cepitis, N. Kongi, J. Rossmeisl and V. Ivanistsev, *ACS Energy Lett.*, 2023, **8**, 1330–1335.
13 H. T. Chung, D. A. Cullen, D. Higgins, B. T. Sneed, E. F. Holby, K. L. More and P. Zelenay, *Science*, 2017, **357**, 479–484.
14 H. Yang, N. Lu, J. Zhang, R. Wang, S. Tian, M. Wang, Z. Wang, K. Tao, F. Ma and S. Peng, *Carbon Energy*, 2023, **5**, e337.
15 P. Cui, L. Zhao, Y. Long, L. Dai and C. Hu, *Angew. Chem., Int. Ed.*, 2023, **135**, e202218269.
16 X. Guo, S. Zheng, Y. Luo and H. Pang, *Chem. Eng. J.*, 2020, **401**, 126005.
17 M. Liu, J. A. Wang, W. Klysubun, G. G. Wang, S. Sattayaporn, F. Li, Y. W. Cai, F. Zhang, J. Yu and Y. Yang, *Nat. Commun.*, 2021, **12**, 5260.
18 K. Wang, K. Yu, S. Xu, S. Yuan, L. Xiang, B. Pang, J. Zheng and N. Li, *Appl. Catal., B*, 2023, **328**, 122445.
19 H. Lei, Q. Wan, S. Tan, Z. Wang and W. Mai, *Adv. Mater.*, 2023, **35**, e2208209.
20 H. Yi, S. Liu, C. Lai, G. Zeng, M. Li, X. Liu, B. Li, X. Huo, L. Qin, L. Li, M. Zhang, Y. Fu, Z. An and L. Chen, *Adv. Energy Mater.*, 2021, **11**, 2002863.
21 S. Yao, X. Zhang, A. Chen, Z. Zhang, M. Jiao and Z. Zhou, *J. Mater. Chem. A*, 2019, **7**, 19290–19296.
22 R. Ma, J. Wang, Y. Tang and J. Wang, *J. Phys. Chem. Lett.*, 2022, **13**, 168–174.
23 K. Yuan, D. Lutzenkirchen-Hecht, L. Li, L. Shuai, Y. Li, R. Cao, M. Qiu, X. Zhuang, M. K. H. Leung, Y. Chen and U. Scherf, *J. Am. Chem. Soc.*, 2020, **142**, 2404–2412.
24 X. Wei, X. Luo, H. Wang, W. Gu, W. Cai, Y. Lin and C. Zhu, *Appl. Catal., B*, 2020, **263**, 118347.
25 R. Lu, C. Quan, C. Zhang, Q. He, X. Liao, Z. Wang and Y. Zhao, *Nano Res.*, 2022, **15**, 6067–6075.
26 Z. Zhang, P. Liu, Y. Song, Y. Hou, B. Xu, T. Liao, H. Zhang, J. Guo and Z. Sun, *Adv. Sci.*, 2022, **9**, e2204297.
27 U. I. Kramm, J. Herranz, N. Larouche, T. M. Arruda, M. Lefevre, F. Jaouen, P. Bogdanoff, S. Fiechter, I. Abs-Wurmbach, S. Mukerjee and J. P. Dodelet, *Phys. Chem. Chem. Phys.*, 2012, **14**, 11673–11688.
28 X. Lu, P. Stepanov, W. Yang, M. Xie, M. A. Aamir, I. Das, C. Urgell, K. Watanabe, T. Taniguchi, G. Zhang, A. Bachtold, A. H. MacDonald and D. K. Efetov, *Nature*, 2019, **574**, 653–657.
29 Y. Cao, V. Fatemi, S. Fang, K. Watanabe, T. Taniguchi, E. Kaxiras and P. Jarillo-Herrero, *Nature*, 2018, **556**, 43–50.

30 A. L. Sharpe, E. J. Fox, A. W. Barnard, J. Finney, K. Watanabe, T. Taniguchi, M. A. Kastner and D. Goldhaber-Gordon, *Science*, 2019, **365**, 605–608.
31 Y. Choi, H. Kim, C. Lewandowski, Y. Peng, A. Thomson, R. Polski, Y. Zhang, K. Watanabe, T. Taniguchi, J. Alicea and S. Nadj-Perge, *Nat. Phys.*, 2021, **17**, 1375–1381.
32 B. H. Solis and S. Hammes-Schiffer, *Inorg. Chem.*, 2014, **53**, 6427–6443.
33 F. Sun, Q. Tang and D.-E. Jiang, *ACS Catal.*, 2022, **12**, 8404–8433.
34 Y. Yu, K. Zhang, H. Parks, M. Babar, S. Carr, I. M. Craig, M. Van Winkle, A. Lyssenko, T. Taniguchi, K. Watanabe, V. Viswanathan and D. K. Bediako, *Nat. Chem.*, 2022, **14**, 267–273.
35 K. Uchida, S. Furuya, J.-I. Iwata and A. Oshiyama, *Phys. Rev. B: Condens. Matter Mater. Phys.*, 2014, **90**, 155451.
36 G. Kresse and J. Furthmüller, *Comput. Mater. Sci.*, 1996, **6**, 15–50.
37 G. Kresse and J. Furthmüller, *Phys. Rev. B: Condens. Matter Mater. Phys.*, 1996, **54**, 11169–11186.
38 J. P. Perdew, K. Burke and M. Ernzerhof, *Phys. Rev. Lett.*, 1996, **77**, 3865–3868.
39 G. Kresse and D. Joubert, *Phys. Rev. B: Condens. Matter Mater. Phys.*, 1999, **59**, 1758–1775.
40 P. E. Blöchl, *Phys. Rev. B: Condens. Matter Mater. Phys.*, 1994, **50**, 17953–17979.
41 S. Grimme, J. Antony, S. Ehrlich and H. Krieg, *J. Chem. Phys.*, 2010, **132**, 154104.
42 J. K. Nørskov, T. Bligaard, A. Logadottir, J. R. Kitchin, J. G. Chen, S. Pandelov and U. Stimming, *J. Electrochem. Soc.*, 2005, **152**, J23–J26.
43 Z. W. Seh, J. Kibsgaard, C. F. Dickens, I. Chorkendorff, J. K. Norskov and T. F. Jaramillo, *Science*, 2017, **355**, eaad4998.

